Biomedical Science Letters 2019, 25(1): 99~106
https://doi.org/10.15616/BSL.2019.25.1.99
eISSN : 2288-7415

Original Article

Classification of ^{18}F-Florbetaben Amyloid Brain PET Image using PCA-SVM

Kook Cho[1,§,], Woong-Gon Kim[3,§,**], Hyeon Kang[1,*], Gyung-Seung Yang[5,**], Hyun-Woo Kim[4,*], Ji-Eun Jeong[1,2,**], Hyun-Jin Yoon[1,2,**], Young-Jin Jeong[1,2,***] and Do-Young Kang[1,2,†,***]**

[1]Institute of Convergence Bio-Health, Dong-A University, Busan 49201, Korea
[2]Department of Nuclear Medicine, Dong-A University Medical Center, Dong-A University College of Medicine, Busan 49201, Korea
[3]Economic Survey, Gyeongin Regional Statistics Office, Gwacheon 13809, Korea
[4]Department of Industrial Engineering, Hanyang University, Seoul 04763, Korea
[5]Ubicod Company, Seoul 08381, Korea

Amyloid positron emission tomography (PET) allows early and accurate diagnosis in suspected cases of Alzheimer's disease (AD) and contributes to future treatment plans. In the present study, a method of implementing a diagnostic system to distinguish β-Amyloid (Aβ) positive from Aβ negative with objectiveness and accuracy was proposed using a machine learning approach, such as the Principal Component Analysis (PCA) and Support Vector Machine (SVM). ^{18}F-Florbetaben (FBB) brain PET images were arranged in control and patients (total n = 176) with mild cognitive impairment and AD. An SVM was used to classify the slices of registered PET image using PET template, and a system was created to diagnose patients comprehensively from the output of the trained model. To compare the per-slice classification, the PCA-SVM model observing the whole brain (WB) region showed the highest performance (accuracy 92.38, specificity 92.87, sensitivity 92.87), followed by SVM with gray matter masking (GMM) (accuracy 92.22, specificity 92.13, sensitivity 92.28) for Aβ positivity. To compare according to per-subject classification, the PCA-SVM with WB also showed the highest performance (accuracy 89.21, specificity 71.67, sensitivity 98.28), followed by PCA-SVM with GMM (accuracy 85.80, specificity 61.67, sensitivity 98.28) for Aβ positivity. When comparing the area under curve (AUC), PCA-SVM with WB was the highest for per-slice classifiers (0.992), and the models except for SVM with WM were highest for the per-subject classifier (1.000). We can classify ^{18}F-Florbetaben amyloid brain PET image for Aβ positivity using PCA-SVM model, with no additional effects on GMM.

Key Words: Alzheimer's disease, Gray matter, β-Amyloid, PCA, SVM, ^{18}F-FBB PET

INTRODUCTION

Alzheimer's disease (AD) is one of the most common causes of dementia among the elderly population and is a progressive and neurodegenerative disease that leads to cognitive impairments, memory loss, and behavioral problems.

β-Amyloid (Aβ) is a typical pathologic feature found in the

Received: December 27, 2018 / Revised: January 14, 2019 / Accepted: January 14, 2019
[*]Graduate student, [**]Researcher, [***]Professor.
[§]These authors contributed equally to this manuscript.
[†]Corresponding author: Do-Young Kang. Department of Nuclear Medicine, Dong-A University Medical Center, Dong-A University College of Medicine, #26 Daesingongwon-ro, Seo-gu, Busan 49201, Korea.
Tel: +82-51-240-5630, Fax: +82-51-242-7237, e-mail: dykang@dau.ac.kr

brain of all patients with AD (Haass et al., 2007; Gunasekaran et al., 2015). Aβ cascade has been postulated to initiate progressive Aβ changes in the brain, leading to neurodegeneration and dementia (Barthel et al., 2011). Therefore, imaging techniques that enable observation of brain Aβ deposition can help in assessing the cortical amyloid burden *in vivo* as well as facilitate early and accurately diagnose AD. Therefore, an amyloid PET, obtained using various radiopharmaceutical modalities, plays an important role in the *in vivo* detection of AD and is also used to identify appropriate therapies as well as diagnose potential AD patients.

^{18}F-Florbetaben (FBB) amyloid PET is one of the types of neuroimaging modalities used to detect Aβ plaque. The physician evaluates the cerebral cortical gray matter uptake in four areas (temporal, occipital, frontal, and parietal regions) of the brain in the axial plane of the ^{18}F-FBB amyloid PET using the brain beta-amyloid plaque load (BAPL) scoring system (1 = no Aβ load, 2 = minor Aβ load, 3 = significant Aβ load) to diagnose whether the case is Aβ-positive or not (Barthel et al., 2011; Lundeen et al., 2018).

However, although the physician's visual assessment of medical images is the most reliable way to evaluate images, it is time-consuming and labor-intensive during image interpretation and prevents physician's goal in reducing the room for inter-observer problems in visually evaluating significant differences of image contrast (Brucher et al., 2015). Therefore, the need for quantitative indicator has been required.

In one aspect of a medical image during signal processing, various studies on improving the discrimination power by appropriately selecting the data characteristics have been conducted. In recent years, several studies have demonstrated the potential of developing biomedical assessment tools to improve the quantification of medical image evaluation using machine learning, such as Support Vector Machine (SVM) or Neural Network, which are used to quantitatively analyze various medical images (Gulshan et al., 2016; Lakhani et al., 2017; Taylor et al., 2017).

In the present study, a predictive model using SVM and a simple rule-based decision that predicts the Aβ-positive and Aβ-negative status were designed. The minor Aβ load characteristics in BAPL 2 can be partially observed in the voxel unit. Therefore, a model was designed to estimate the posterior probability of Aβ-positive slices at the axial plane resampled (15~50th) from voxels to mimic the clinical practice. The performances before and after gray matter masking (GMM) were also compared.

Table 1. Demographic details of the subjects used for the experiment

Characteristics	BAPL* 1	BAPL 2	BAPL 3	Total
No. of patients	60	53	60	173
Mean (SD) of age	67.55 (9.01)	73.02 (5.64)	69.08 (8.83)	69.76 (8.33)
No. slice of Aβ-negative	2,160	931	0	3,091
No. slice of Aβ-positive	0	977	2,160	3,137

*BAPL: brain β-amyloid plaque load

MATERIALS AND METHODS

Subjects

An experiment on the retrospective cohort in the Department of Nuclear Medicine, Dong-A University Medical Center (DANM), was conducted from November 2015 to May 2018. The total number of subjects in the cohort was 173, which consisted of 60 subjects with BAPL scores of 1 (BAPL 1), 53 with BAPL scores of 2 (BAPL 2), and 60 with BAPL scores of 3 (BAPL 3). Therefore, according to the definition of the BAPL scoring system, images from 60 subjects who were negative for Aβ and 113 subjects who were positive for Aβ were used to train and validate our predictive model. Specific details of the study populations are shown in Table 1.

Labeling and sampling

All evaluated clinical diagnoses of ^{18}F-FBB PET images and BAPL scores in the DANM dataset were organized in cooperation with the Department of Neurology, Dong-A University Medical Center. All images of subjects used in this study were evaluated on the same criteria; regional cortical tracer uptake (RCTU) (1, no tracer uptake; 2, moderate tracer uptake; 3, pronounced tracer uptake) and BAPL scoring system. RCTU score is decided according to the uptake state of gray matter and white matter in four regions; frontal cortex,

lateral temporal cortex, posterior cingulate cortex/precuneus, and parietal cortex. The BAPL score of a subject is finally determined by combining the results of the RCTU score by region (Seibyl et al., 2016; Bullich et al., 2017). According to the current diagnostic criteria for ^{18}F-FBB PET image (Piramal Imaging Limited, 2014), BAPL 1 is considered Aβ-negative, and BAPL 2 and BAPL 3 are considered Aβ-positive. And such a decision depends on the physician's visual assessment of each slice on the axial plane. Therefore, the slices were respectively indexed in the axial plane for all dataset, and one physician from the DANM performed the visual assessment after sampling the pre-determined slices (a total of 36 slices from 15th to 50th slices).

The Nested Cross Validation (NCV) was used as a performance estimation scheme to validate the hyper-parameter of a model and test it using the entire dataset (Varma et al., 2006). In addition, cluster bootstrapping was performed to preserve patient independence during the sampling phase (Sherman et al., 2007) and stratified sampling for each subset to obtain an almost similar distribution for the per-subject BAPL score groups during the sampling process for the NCV. The number of folds was determined as observable performance variables while maintaining an appropriate variance in the limited dataset; therefore, four-fold NCV was selected as the final scheme for performance estimation.

Data pre-processing

The final Aβ PET images obtained from the scanner and given to a physician for the diagnosis measured 400×400 ×110 (height × width × depth) with a thickness of 1.09 ×1.09×1.5 (mm). Before fitting the selected machine learning function to the PET dataset, a classic preprocessing was performed to make the functional characteristics of the brain prominent in minimized morphological and anatomical differences between the patient and the normal scan. First, we made a ^{18}F-FBB PET template through an average of 21 NC and 9 AD subjects who imaged ^{18}F-FBB Amyloid PET in DANM. Moreover, all datasets were mapped on the same template space. Finally, count normalization function was applied for each dataset. The above preprocessing, which applies the same data individually, was performed using MATLAB (Version 9.4, 0.813654) and Statistical Parametric Mapping (SPM8) module. The result images obtained from SPM8 have three-dimensional voxels size of 95×79×68 with a thickness of 2×2×2 (mm).

We also considered GMM, obtained from the PET template used for spatial normalization, as well as the whole brain (WB) volume. Detailed appearance and characteristics for acquired ^{18}F-FBB PET and PET template have been shown in our previous study (Kang et al., 2018).

In general, classification problems, including image recognition fields, can be subdivided into feature extraction and classification problems; therefore, these are mainly applied in the medical field (Gonçalves et al., 2016; Xue et al., 2016; Segovia et al., 2018). Feature extraction was attempted using Principal Component Analysis (PCA) prior to solving the classification problem using SVM.

This feature extraction was performed outside the outer and inner loops of the NCV, in which the inner loop operates a wrapper algorithm that searches hyper-parameters by performing the holdout again on the subset from the entire dataset for hyper-parameter validation, such as grid search or random search algorithm (Pedregosa et al., 2011; Bergstra et al., 2012; Taylor et al., 2017). In this work, Bayesian optimization (Snoek et al., 2012) was used as the wrapper algorithm. In each outer loop, the hyper-parameter ultimately determined from each inner loop was used to select the best model in estimating the generalization performance (Varma and Simon, 2006). All source codes for data preprocessing after spatial normalization were written in packages implemented using Python and scikit-learn, a set of machine learning library (Python 3.5.2, scikit-learn 0.19.1).

Support vector machine

Since other classifiers, such as neural networks, are designed to minimize the error rate, SVM has shown high generalization performance by searching for a decision boundary that maximizes the margin between two classes (Vapnik et al., 1998; Oh et al., 2008).

In order to classify the preprocessed amyloid PET voxel data, the SVM was selected in our experiment, the hyper-parameters were searched through a Bayesian optimizer, and validation phase was performed in the inner loop of the NCV. The generalization performance of the model whose

Table 2. Comparison of performance according to features used for discrimination (%)

Features	Per-slice performance			Per-subject performance		
	Accuracy	Specificity	Sensitivity	Accuracy	Specificity	Sensitivity
PCA-SVM, WB*	92.38	92.87	92.03	89.21	71.67	98.28
PCA-SVM, GM*	92.00	91.34	92.44	85.80	61.67	98.28
SVM, WB	91.03	91.67	90.59	82.39	58.33	94.83
SVM, GM	92.22	92.13	92.28	82.96	53.33	98.28

*PCA: principle component analysis, *SVM: support vector machine, *WB: whole brain, *GM: gray matter

hyper-parameter was determined in the inner loop was estimated in the outer loop of the NCV. The hyper-parameter space searched using the Bayesian optimizer was Kernel, a categorical variable (among "linear", "rbf", and "poly"); C, the strength of penalty (from 1 to 1e + 2); gamma, a parameter for Gaussian kernel: Radial Basis Function (RBF) (from 1e-4 to 1e-1); and the number of features from PCA (from 10 to 5,000). Before statistically estimating the Bayesian optimization, the initial candidate was arbitrarily determined by the practitioner as "linear" for the type of kernel, 1 for C, 1 for gamma, and 100 for the number features from PCA. Specific details are presented in Table 2. The number of searches for one inner loop, validation phase to search for a better hyper-parameter, was 20 times, and the expected improvement was used to acquire functions during Bayesian optimization (Moćkus et al., 1978).

In the present study, the per-slice posterior probability for each sample was ultimately estimated to be Aβ-positive and per-subject posterior probability to be Aβ-positive using the selected SVM model (Platt et al., 1999). After estimating the per-slice Aβ-positive, our system calculates per-slice predictions based on the 36 per-slice probabilities to be Aβ-positive per person by mimicking the clinical practice decisions. Here if at least one of the 36 slices showed Aβ-positive result, the subject was assigned as Aβ-positive. The performances, such as accuracy, sensitivity, and specificity are estimated using 50% of the cutoff for Aβ-positive.

Statistical analysis

The data collected and used in this experiment were summarized and analyzed using MedCalc version 18.9.1 (MedCalc Software). The scores, posterior probabilities estimated from PCA-SVM and SVM for Aβ positivity were used to estimate the receiver operating characteristic (ROC) curve and area under curve (AUC) analysis and were compared using a theory developed for generalized U-statistics (DeLong et al., 1988). Continuous variables estimated through the NCV (performances of selected model and hyper-parameter candidates such as C, gamma, and number features of PCA) were tested for normality through the Shapiro-Wilk test. Statistical comparison results were performed by considering the significance level of 0.05.

RESULTS

Each value shown in Table 2 was the average of each performance estimated from the outer loop of four-fold NCV according to the observed brain region and evaluation standards as per-slice or per-subject. To compare the per-slice classification, the PCA-SVM with WB showed the highest performance (accuracy 92.38, specificity 92.87, sensitivity 92.87), followed by SVM with GMM (accuracy 92.22, specificity 92.13, sensitivity 92.28) for Aβ positivity. On the contrary, when comparing according to per-subject classification, the PCA-SVM WB also showed the highest performance (accuracy 89.21, specificity 71.67, sensitivity 98.28), followed by PCA-SVM with GMM (accuracy 85.80, specificity 61.67, sensitivity 98.28) for Aβ positivity.

When comparing the ROC curve at per-slice standard, PCA-SVM with WB shows the largest AUC (0.992, 95% CI: 0.985~0.996), followed by PCA-SVM with GMM (0.990, 95% CI: 0.984~0.995) for Aβ positivity. On the contrary, the AUCs at per-subject standard were highest in PCA-SVM with WB, PCA-SVM with GMM, and SVM with GMM

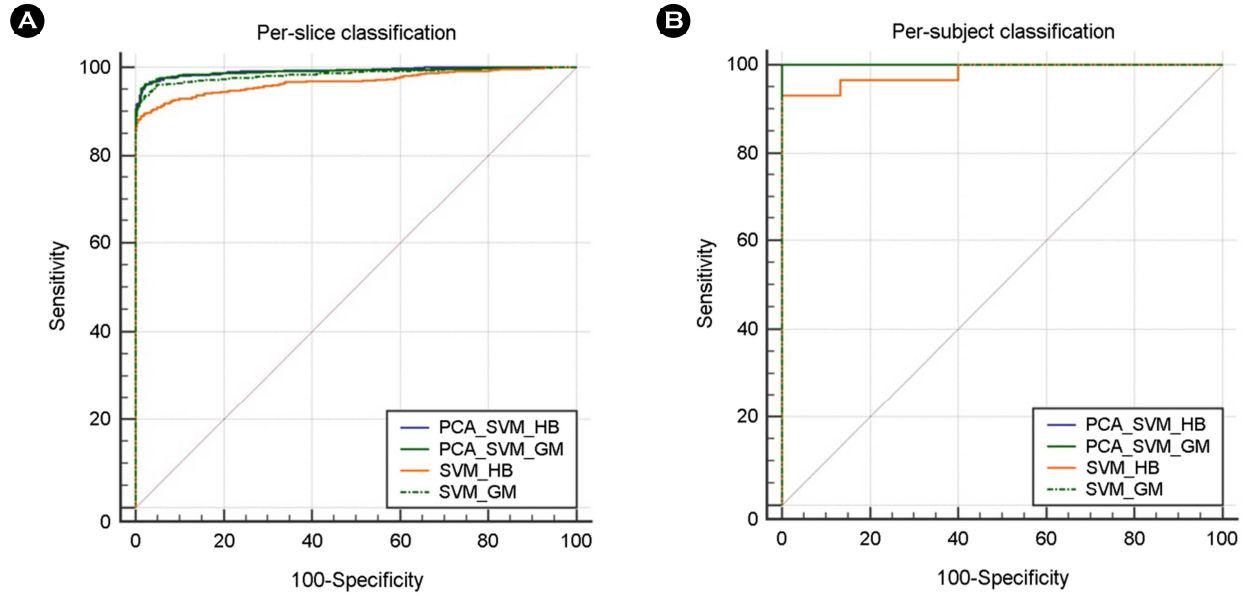

Fig. 1. Receiver operating characteristic (ROC) analysis to classify several experiments. (A) and (B) show the comparison of ROC curve according to their discrimination power at per-slice and per-subject standard, respectively. In Fig. 1-A, each of area under curve (AUC) were PCA_SVM_HB (0.992, 95% CI: 0.985~0.996), PCA_SVM_GM (0.990, 95% CI: 0.984~0.995), SVM_HB (0.967, 95% CI: 0.956~0.976), and SVM_GM (0.985, 95% CI: 0.976~0.991), and in Fig. 1-B, each of them were PCA_SVM_HB (1.000, 95% CI: 0.920~1.000), PCA_SVM_GM (1.000, 95% CI: 0.920~1.000), SVM_HB (0.982, 95% CI: 0.887~1.000), and SVM_GM (1.000, 95% CI: 0.920~1.000). The pairwise comparison of ROC curves is shown in Table 3.

Table 3. Pairwise comparison of ROC curves for each model at each standard

Comparisons	Per-slice (DBA*, *P*-value)	Per-subject (DBA, *P*-value)
PCA-SVM, WB ~ PCA-SVM, GM**	0.0013, *P* = 0.3019	0.0000, *P* = 1.0000
PCA-SVM, WB ~ SVM, WB**	0.0249, *P* < 0.0001	0.0184, *P* = 0.2354
PCA-SVM, WB ~ SVM, GM	0.0072, *P* = 0.0010	0.0000, *P* = 1.0000
PCA-SVM, GM ~ SVM, WB	0.0236, *P* < 0.0001	0.0184, *P* = 0.2454
PCA-SVM, GM ~ SVM, GM	0.0059, *P* = 0.0001	0.0000, *P* = 1.0000
SVM, WB ~ SVM, GM	0.0177, *P* < 0.0001	0.0184, *P* = 0.2454

*DBA: difference between areas
**PCA: principle component analysis, **SVM: support vector machine, **WB: whole brain, **GM: gray matter

(1.000, 95% CI: 0.920~1.000), respectively, followed by SVM with WB (0.982, 95% CI: 0.887~1.000). Specific details of ROC curves in this study are shown in Fig. 1.

The pairwise comparison results of the ROC curves for each experimental model are shown in Table 3. On the pairwise comparison at the per-slice standard, the differences in the AUCs between the SVM with WB and other three models (PCA-SVM with WB, PCA-SVM with GM, and SVM with GM) were the most significant, respectively (0.0249, *P* < 0.0001; 0.0236, *P* < 0.0001; 0.0177, *P* < 0.0001), followed by PCA-SVM with GM ~ SVM with GM (0.0059, *P* = 0.0001) and PCA-SVM with WB ~ SVM with GM (0.0072, *P* = 0.0010). PCA-SVM with WB ~ PCA-SVM with GM showed no significant differences (0.0013, *P* = 0.3019). However, no significant differences were observed at per-subject standard in all cases.

Hyper-parameters ultimately determined from each inner loop of the NCV through the Bayesian optimizer and used to estimate per-slice classification performance are summarized in Table 4. Regardless of the experimental model, the poly-

Table 4. Hyper-parameter statistics searched by Bayesian optimization after each inner loop

Item	PCA-SVM**		SVM		Total
	WB**	GM**	WB	GM	
Kernel*	3:0:13	5:0:11	3:0:13	5:0:11	16:0:48
C	23.57 (27.79)	25.17 (29.35)	31.53 (38.22)	25.47 (32.92)	26.43 (31.69)
Gamma	0.0089 (0.0090)	0.0228 (0.0368)	0.0306 (0.0506)	0.0364 (0.0471)	0.0247 (0.0398)
No. PCA feature	2,334 (1,331)	1,720 (1,552)	−	−	2,027 (1,456)
Accuracy (%) (SD)	94.99 (2.36)	94.25 (2.45)	93.75 (2.07)	93.46 (3.11)	94.11 (2.53)
95 % CI	93.84~96.15	93.05~95.45	92.73~94.77	91.94~94.98	93.49~94.73

*Kernel: selected kernel as categorical variable (linear: radial basis; function: polynomial)
**PCA: principle component analysis, **SVM: support vector machine, **WB: whole brain, **GM: gray matter

nomial kernel was most commonly adopted, followed by linear kernel. In addition, the RBF kernel was not adopted even once in all cases (linear:RBF:polynomial = 16:0:48), and the validation performance on each inner loop in the NCV was estimated. The hyper-parameter of these experiments as continuous variables such as C, gamma, and number features of PCA estimated through the NCV were denied normality by Shapiro-Wilk test but their performance distribution was accepted as normality.

DISCUSSION

Because of the pathological nature of AD, the diagnosis of subject's brain must be taken into account in stereotactic coordinates. In order to analyze the 3-dimensional information of a object, there is a study in which an approach to extract the feature from the 3-dimensional voxel data of a sample is applied to the brain (Zhang et al., 2011; Blanc-Durand et al., 2017). Because these studies do not provide information per slices, there is a limit to providing information that is sympathetic to physicians and patients.

In order to create a model that performs the per-slice classification, only visually determined per-slice BAPL 2 in the per-subject BAPL 2 group were considered as dataset to fit and test a model, and visually determined per-slice BAPL 1 included in the per-subject BAPL 2 group were not used as the dataset. Regarding the methods used during the experiment to determine the subject's Aβ deposition status, even a single misclassification may have had a large impact on the specificity. Therefore, specificity was lower than sensitivity in Table 2. In order to improve this specificity, other rules to test per-subject discrimination should be implemented.

In a conventional quantitative analysis of amyloid PET according to the pathological deposition patterns of the amyloid plaque, studies have considered the gray matter as the region of interest (Choi et al., 2016). On the per-slice classification shown in Table 3, because the pairwise comparisons show significant differences in both cases that used PCA-SVM, the feature seems to be extracted using the PCA per-slice. In addition, in cases that did not use PCA, the performance of SVM with GMM was significantly improved. Moreover, the model with PCA showed no significant performance improvement according to WB and GM. Thus, PCA and WB can extract features with a similar discrimination level.

The results of hyper-parameter determined in the inner loop showed a validation performance that was slightly higher than that of the generalization. Therefore, SVM seems to be able to show the best performance, while compromising the performance properly instead of falling into overfitting. The performance estimates shown in the inner loop of the NCV for each experimental model followed the normal distribution and showed a somewhat constant CI, unlike the distribution of the hyper-parameters. In the quantitative analysis of ^{18}F-FBB images, the dataset to be fitted seems to be more important than the influence of the hyper-parameters in the selected model.

There were several machine learning techniques and amyloid radiotracers for detection of Alzheimer's disease. 18F FDG PET imaging was used for computer aided Alzheimer's

diagnosis. By SVM, the 88.24% accuracy in identifying mild AD, with 88.64% specificity, and 87.70% sensitivity is obtained (Illán IA et al., 2011). A computer aided diagnosis (CAD) system for the Alzheimer's disease detection was performed with a 18F-FDG and Pittsburg Compound B (PiB) PET. In the first, FDG results got better reaching an accuracy of 94.74%, in the second set both FDG and PIB rates were improved reaching a maximum accuracy of 92.86% (Chaves et al., 2012).

CONCLUSIONS

We create SVM model to estimate the posterior probabilities to be Aβ-positive for each slices of a subject. And the posterior probabilities for each subject were estimated using the calculated per-slice posterior probabilities and we evaluated the performance of our model according to brain region and use of PCA. The data set used in the experiment was 173 subject imaged ^{18}F-FBB PET. The results of this experiment showed that the per-slice classification with PCA shows better performance to classify Aβ-positive and Aβ-negative groups. And GM in the axial plane can be a feature that helps discriminate between Aβ-positive and Aβ-negative group for quantitative analysis using machine learning.

ACKNOWLEDGEMENT

This research was supported by the National Research Foundation (NRF) funded by the Ministry of Science, ICT & Future Planning (NRF-2018R1A2B2008178).

CONFLICT OF INTEREST

No potential conflict of interest relevant to this article was reported.

REFERENCES

Barthel H, Gertz HJ, Eresel S, Peters O, Bartenstein P, Buerger K, Hiemeyer F, Wittmer-Rump SM, Seibyl J, Reininger C, Sabri O. Cerebral amyloid-β PET with florbetaben (18F) in patients with Alzheimer's disease and healthy controls: a multicenter phase 2 diagnostic study. The Lancet Neurology. 2011. 10: 424-435.

Bergstra J, Bengio Y. Random search for hyper-parameter optimization. Journal of Machine Learning Research. 2012. 13: 281-305.

Blanc-Durand P, Van Der Gucht A, Guedj E, Abulizi M, Aoun-Sebaiti M, Lerman L, Verger A, Authier FJ, Itti E. Cerebral 18F-FDG PET in macrophagic myofasciitis: An individual SVM-based approach. PloS One. 2017. 12: e0181152.

Brucher N, Mandegaran R, Filleron T, Wagner T. Measurement of inter- and intra-observer variability in the routine clinical interpretation of brain 18-FDG PET-CT. Annals of Nuclear Medicine. 2015. 29: 233-239.

Bullich S, Seibyl J, Catafau AM, Jovalekic A, Koglin N, Barthel H, Sabri O, Santi SD. Optimized classification of ^{18}F-Florbetaben PET scans as positive and negative using an SUVR quantitative approach and comparison to visual assessment. NeuroImage Clinical. 2017. 15: 325-332.

Chaves R, Ramírez J, Górriz JM, Illán IA, Salas-Gonzalez D. FDG and PIB biomarker PET analysis for the Alzheimer's disease detection using Association Rules. IEEE Nuclear Science Symposium and Medical Imaging Conference Record. 2012. s2576-2579.

Choi WH, Um YH, Jung WS, Kim SH. Automated quantification of amyloid positron emission tomography: a comparison of PMOD and MIMNEURO. Annals of Nuclear medicine. 2016. 30: 682-689.

DeLong ER, DeLong DM, Clarke-Pearson KL. Comparing the areas under two or more correlated receiver operating characteristic curves: a nonparametric approach. Biometrics. 1988. 44: 837-845.

Gonçalves AB, Souza JS, da Silva GG, Cereda MP, Pott A, Naka MH, Pistori H. Feature extraction and machine learning for the classification of Brazilian savannah pollen grains. PloS One. 2016. 11: e0157044.

Gulshan V, Peng L, Coram M, Stumpe MC, Wu D, Narayanaswamy A, Kim R. Development and validation of a deep learning algorithm for detection of diabetic retinopathy in retinal fundus photographs. Jama. 2016. 316: 2402-2410.

Gunasekaran TI, Ohn T. MicroRNAs as Novel Biomarkers for the Diagnosis of Alzheimer's Disease and Modern Advancements in the Treatment. Biomedical Science Letters. 2015. 21: 1-8.

Haass C, Selkoe DJ. Soluble protein oligomers in neurodegeneration: lessons from the Alzheimer's amyloid β-peptide. Nature Reviews Molecular Cell Biology. 2007. 8: 101.

Illán IA, Górriz JM, Ramírez J, Salas-Gonzalez D, López MM,

Segovia F, Chaves R, Gómez-Rio M, Puntonet CG. The Alzheimer's Disease Neuroimaging Initiative. 18F-FDG PET imaging analysis for computer aided Alzheimer's Diagnosis. 2011. 181: 903-916.

Kang H, Kim WG, Yang GS, Kim HW, Jeong JE, Yoon HJ, Cho K, Jeong YJ, Kang DY. VGG-based BAPL score classification of ^{18}F-Florbetaben Amyloid Brain PET. J Exp Biomed Sci. 2018.

Lakhani P, Sundaram B. Deep learning at chest radiography: automated classification of pulmonary tuberculosis by using convolutional neural networks. Radiology. 2017. 284: 574-582.

Lopresti BJ, Klunk WE, Mathis CA, Hoge JA, Ziolko SK, Lu X, Price JC. Simplified quantification of Pittsburgh Compound B amyloid imaging PET studies: a comparative analysis. Journal of Nuclear Medicine. 2005. 46: 1959-1972.

Lundeen TF, Seibyl JP, Covington MF, Eshghi N, Kuo PH. Signs and artifacts in Amyloid PET. Radio Graphics. 2018. 38: 2123 -2133.

Moćkus J, Tiesis V, Źilinskas A. The Application of Bayesian Methods for Seeking the Extremum: Toward global optimization 2. 1978. pp 117. Elsevier. Amsterdam, Netherlands.

Oh IS. Pattern recognition. 2008. pp 137-173. Kyobobook. Seoul, Korea.

Pedregosa F, Varoquaux G, Gramfort A, Michel V, Thirion B, Grisel O, Blondel M, Prettenhofer P, Weiss R, Dubourg V, Vanderplas J, Passos A, Cournapeau D. Scikit-learn: machine learning in python. Journal of Machine Learning Research. 12: 2825-2830.

Piramal Imaging Limited. Neuraceq. Summary of product characteristics. Cambridge: Piramal Imaging Limited. 2014.

Platt J. Probabilistic outputs for support vector machines and comparisons to regularized likelihood methods. Advances in Large Margin Classifiers. 1999. 10: 61-74.

Segovia F, Sánchez-Vañó R, Górriz JM, Ramírez J, Sopena-Novales P, Dardel NT, Gómez-Río M. Using CT data to improve the quantitative analysis of ^{18}F-FBB PET neuroimages. Frontiers in Aging Neuroscience. 2018. 10: 158.

Seibyl J, Catafau AM, BARthel H, Ishii K, Rowe CC, Leverenz JB, Ghetti B, Ironside JW, Takao M, Akatsu H, Murayama S, Bullich S, Mueller A, Koglin N, Schulz-Schaeffer WJ, Hoffmann A, Sabbagh MN, Stephens AW, Sabri O. Impact of training method on the robustness of the visual assessment of ^{18}F-Florbetaben PET scan: results from a phase-3 study. J Nucl Med. 2016. 57: 900-906.

Sherman M, Cessie SL. A comparison between bootstrap methods and generalized estimating equations for correlate outcomes in generalized linear models. Communications in Statistics-Simulation and Computation. 1997. 26: 901-925.

Snoek J, Larochelle H, Adams RP. Pracical Bayesian optimization of machine learning algorithm. In Advances in Neural Information Processing System. 2012. 2951-2959.

Taylor JC, Fenner JW. Comparison of machine learning and semi-quantification algorithms for (I123) FP-CIT classification: the beginning of the end for semi-quantification?. EJNMMI Physics. 2017. 4: 29.

Vapnik VN. 10.5 Support Vector Machine: Statistical Learning Theory. 1998. pp 421-441. Wiley-Interscience. Hoboken, USA.

Varma S, Simon R. Bias in error estimation when using cross-validation for model selection. BMC Bioinformatics. 2006. 7: 91.

Xue DX, Zhang R, Feng H, Wang YL. CNN-SVM for microvascular morphological type recognition with data augmentation. Journal of Medical and Biological Engineering. 2016. 36: 755 -764.

Zhang Y, Dong Z, Wu L, Wang S. A hybrid method for MRI brain image classification. Expert Systems with Applications. 2011. 38: 10049-10053.

https://doi.org/10.15616/BSL.2019.25.1.99

Cite this article as: Cho K, Kim WG, Kang H, Yang GS, Kim HW, Jeong JE, Yoon HJ, Jeong YJ, Kang DY. Classification of ^{18}F-Florbetaben Amyloid Brain PET Image using PCA-SVM. Biomedical Science Letters. 2019. 25: 99-106.